ACS APPLIED MATERIALS & INTERFACES

Research Article

www.acsami.org

Efficient and Stable Red Emissive Carbon Nanoparticles with a Hollow Sphere Structure for White Light-Emitting Diodes

Yi Fan,[†] Xiaoyang Guo,*[,†] Yongqiang Zhang,[†,‡] Ying Lv,[†] Jialong Zhao,[$] and Xingyuan Liu*[,†]

[†]State Key Laboratory of Luminescence and Applications, Changchun Institute of Optics, Fine Mechanics and Physics, Chinese Academy of Sciences, Changchun 130033, China

[‡]University of Chinese Academy of Sciences, Beijing 100039, China

[$]Key Laboratory of Functional Materials Physics and Chemistry of the Ministry of Education, Jilin Normal University, Siping 136000, China

S *Supporting Information*

ABSTRACT: Red-emissive solid-state carbon nanoparticles (CNPs) with a hollow sphere structure for white light-emitting diodes (WLEDs) were designed and synthesized by molecular self-assembly and microwave pyrolysis. Highly ordered graphite-like structures for CNPs were characterized by transmission electron microscopy, X-ray photoelectron spectroscopy, and ultraviolet−visible (UV−vis) spectroscopy. The emission mechanism of the red-emissive solid-state CNPs was investigated in detail by steady-state and time-resolved photoluminescence (PL) spectroscopy. The as-prepared CNPs showed a red emission band centered at 620 nm with excitation wavelength independence, indicating uniform size of sp^2 carbon domains in the CNPs. The CNPs also had a PL quantum yield (QY) of 17% under 380 nm excitation. Significantly, the PL QY of the organosilane-functionalized CNPs was 47%, which is the highest value recorded for red-emissive solid-state carbon-based materials under UV-light excitation. More importantly, the red-emissive CNPs exhibited a PL QY of 25% after storage in air for 12 months, indicating their excellent stability. The red-emissive CNP powders were used as environmentally friendly and low-cost phosphors on a commercial 460 nm blue GaN-based chip, and a pure white light with CIE coordinates of (0.35, 0.36) was achieved. The experimental results indicated that the red-emissive CNP phosphors have potential applications in WLEDs.

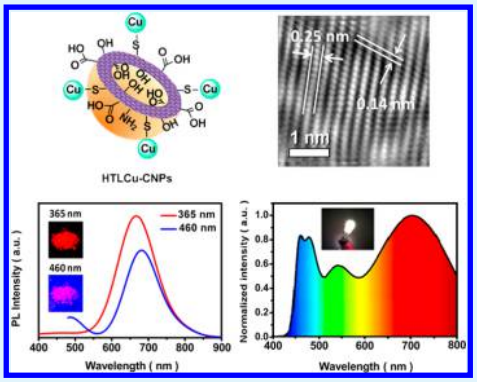

KEYWORDS: *carbon nanoparticles, white light-emitting diodes, red emission, self-assembly, excitation wavelength-independent photoluminescence*

1. INTRODUCTION

Carbon nanoparticles (CNPs) have recently emerged as important fluorescent nanomaterials due to their attractive properties, including low cost, good biocompatibility, easy surface modification, rich colors, and excitation wavelength-dependent photoluminescence (PL) behaviors.[1] These characteristics make CNPs useful in a variety of applications, such as in white light-emitting diodes (WLEDs),[2,3] bioimaging,[4] printing inks,[5,6] photocatalysis,[7] solar cells,[8,9] and sensors.[10] Many blue-[11,12] and green-emissive[13,14] CNP solutions have been reported, and the highest reported PL quantum yields (QYs) from band edge or surface groups are more than 80 and 50%, respectively. However, as a novel kind of environmentally friendly luminescent material, the lack of red-emissive CNPs, especially red-emissive solid-state CNP phosphors, greatly impedes their application, especially in solid-state lighting and displays.

According to the literature, there are two distinct limitations to currently available red-emissive solid-state CNPs. First, theoretical calculations have demonstrated that the emission wavelength of CNPs is dependent on the actual size of the sp^2 carbon domains,[15] which means the real domination of the quantum confinement effect. The actual size of sp^2 carbon domains of CNPs is difficult to accurately control because of numerous precursors, various synthesis approaches, and diverse reactions. To achieve red-emissive CNPs, several methods have been developed. It has been found that the PL wavelength of CNP solutions can be shifted to longer wavelengths by increasing the photon reabsorption,[16] polyethylenimine (PEI) modification,[17] modifying the reaction time[10] or π-conjugation degree,[18] substituting group position,[19] or surface-metal cation functionalization.[20] However, the emission wavelength of CNPs, which is dependent on the excitation wavelength, cannot be accurately controlled. Therefore, yellow- or red-emissive CNPs with lower QYs are always mixed with blue- or green-emissive CNPs, and they need to be separated by tedious

Received: August 25, 2016
Accepted: November 3, 2016
Published: November 3, 2016

DOI: 10.1021/acsami.6b10654
ACS Appl. Mater. Interfaces 2016, 8, 31863−31870

Table 1. Fluorescence Lifetimes of SiHTLCu-CNPs and SiHTLCu-CNPs Stored in Air for 12 Months

sample	τ_1 (μs)	A_1 (%)	τ_2 (μs)	A_2 (%)	X^2	τ_{aver} (μs)	QY (%)
SiHTLCu-CNPs	0.80	9.04	16.94	90.44	0.9997	16.86	47
SiHTLCu-CNPs at 12 months	9.21	39.42	2.04	60.57	0.9981	7.39	25

Scheme 1. Schematic Diagram for the Synthesis of HTLCu-CNPs

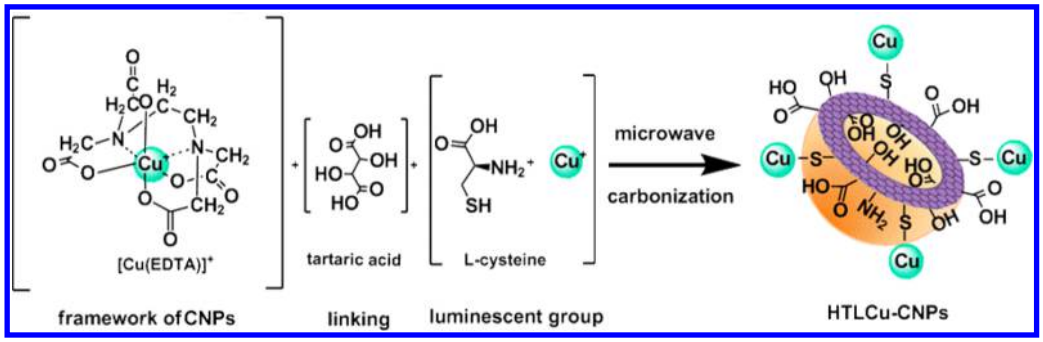

and special methods.[21−24] For example, Ding et al. reported the efficient separation of red-emissive CNPs in water solution (centered at 625 nm, PL QY of 24% under 365 nm excitation) via silica column chromatography.[23] Second, most CNPs show strong fluorescence in dilute solutions, but there is significant aggregation-induced fluorescence quenching[25,26] which limits the use of CNPs in solid-state lighting, displays, biodetection, and so on. To prevent the aggregation-induced fluorescence quenching of CNPs, researchers usually use organosilane-functionalized CNPs[27] or mix the CNPs with polymers such as poly(vinyl alcohol) (PVA),[19,28] poly(methyl methacrylate) (PMMA),[29] polyethylene glycol (PEG),[30,31] and starch.[20] Jiang et al. reported efficient red-emissive CNPs in ethanol solution (centered at 603 nm, PL QY of 20.6%) prepared from *p*-phenylenediamine, but the QY of the CNPs in PVA film was not reported.[19] Bhunia reported efficient red-emissive CNPs in water (centered at 600 nm, PL QY of 7%), but the QY of the CNP powders was not mentioned.[32] Qu reported efficient red-emissive CNPs in dilute ethanol solution with a PL QY of 46% under 540 nm excitation (centered at 580 nm), whereas their starch/CNP phosphors showed a reduced PL QY of 23% under 540 nm excitation.[20] Among all the reported red-emissive CNPs, the fabrication of efficient solid-state CNPs with red emission under 460 nm excitation has not been reported yet. Therefore, the development of efficient and stable red-emissive solid-state CNPs will have a significant impact on the application of CNPs.

Herein, ultraviolet (UV) light-excited red-emissive solid-state CNPs with a hollow sphere structure were strategically designed and synthesized for WLEDs by molecular self-assembly and microwave pyrolysis. The emission mechanism of the red-emissive solid-state CNPs was explored in detail by steady-state and time-resolved PL spectroscopy. The PL properties and stability of as-prepared CNPs with a red emission of 620 nm under 380 nm light excitation were studied. Red-emissive solid-state organosilane-functionalized CNPs were used to fabricate environmentally friendly and low-cost WLEDs based on a 460 nm emissive GaN-based chip. A pure white light with CIE coordinates of (0.35, 0.36) was achieved, indicating that red-emissive solid-state CNPs have potential applications in commercial WLEDs.

2. EXPERIMENTAL SECTION

2.1. Materials. *N*-(2-Hydroxyethyl)ethylenediamine-*N*,*N*′,*N*′-triacetic acid (HEDTA) was purchased from Tokyo Chemical Industry Co., Ltd. L-cysteine, tartaric acid, and glycine were purchased from Sinopharm Chemical Reagent Co., Ltd. Tetraethyl orthosilicate (TEOS), CuCl, $CuCl_2$, $MnCl_2$, $FeCl_2$, $FeCl_3$, $CdCl_2$, $ZnCl_2$, and $AgNO_3$ were purchased from Beijing Chemical Works. All chemicals were used without further purification. The water used in all experiments was purified with a Millipore II system.

2.2. Synthesis of Red-Emissive Solid-State CNPs. In a typical process, red-emissive solid-state CNPs were prepared through microwave treatment of the original materials. First, 4 mmol of tartaric acid and 3 mmol of HEDTA were added to 15 mL of water. After the mixture was stirred for 15 min at 40 °C, 4 mmol of L-cysteine and 0.2 mL of hydrochloric acid were added. Then, 2 mmol of CuCl was added to the solution with vigorous stirring. Finally, the precursor solution was treated at middle high power in a microwave oven for 3 min. The excess original materials were removed by washing original materials with ethanol and acetone three times. Finally, the formed product was dried in a vacuum drying oven at 60 °C for 72 h and stored at room temperature for future characterization and use. The red-emissive solid-state CNPs are denoted as HTLCu-CNPs.

2.3. Synthesis of Green-Emissive CNPs. Green-emissive solid-state CNPs were also prepared by the microwave method. Typically, glycine (8 mmol) and HEDTA (2 mmol) were added to 15 mL of deionized water and stirred for 15 min at 50 °C. The precursor was treated at middle high power in a microwave oven for 3 min. The residue was removed by washing the product three times with acetone and ethanol. Finally, the formed product was dried in a vacuum drying oven at 60 °C for 72 h.

2.4. Synthesis of SiHTLCu-CNPs. Four mmol of tartaric acid, 3 mmol of HEDTA, 4 mmol of L-cysteine, 0.5 mL of CuCl solution, and 1.5 mL of TEOS were ground together. The mixture was then treated on middle high power in a microwave oven for 3 min.

2.5. Preparation of WLEDs. For the fabrication of WLEDs, LED lamps with a peak wavelength centered at 460 nm were used. The devices were made by coating CNPs encased in superglue on a prototype LED unit composed of a 460 nm GaN-based light-emitting chip.

2.6. Characterization. Transmission electron microscopy (TEM) images were recorded with a FEI-TECNAI G2 F30 transmission electron microscope operating at 200 kV. Fourier transform infrared (FTIR) spectra were recorded using KBr tablets with a Bio-Rad Excalibur FTS3000 spectrometer (4000−1000 cm^{-1}). The X-ray photoelectron spectroscopy (XPS) measurements were performed on Thermo ESCALAB 250 using monochromatized Al Kα ($h\nu$ = 1486.8 eV) excitation. A Shimadzu UV-3101 spectrophotometer was used to measure the UV−vis absorption spectra. An F-7000 Hitachi

DOI: 10.1021/acsami.6b10654
ACS Appl. Mater. Interfaces 2016, 8, 31863−31870

fluorescence spectrometer was used to record the PL emission spectra. The PL QYs were obtained in a calibrated integrating sphere in FLS920 spectrometer. Fluorescence lifetimes were measured using an FLS920 time-corrected single-photon counting system. The color coordinates and CCT of the WLEDs were measured on an Ocean optics USB-4000 spectrometer.

2.7. Lifetime Measurements. The decay traces for the CNPs were fitted using a double-exponential function, $Y(t)$, based on nonlinear least-squares analysis in eq 1.

$$Y(t) = \alpha_1 \exp(-t/\tau_1) + \alpha_2 \exp(-t/\tau_2) \quad (1)$$

where α_1 and α_2 are the fractional contributions of decay lifetimes τ_1 and τ_2, respectively. The average lifetimes were calculated using eq 2[33] as follows:

$$\bar{\tau} = \frac{\alpha_1 {\tau_1}^2 + \alpha_2 {\tau_2}^2}{\alpha_1 \tau_1 + \alpha_2 \tau_2} \quad (2)$$

The results are summarized in Table 1.

3. RESULTS AND DISCUSSION

3.1. Design of CNP Synthesis. In this work, a highly efficient synthesis strategy to construct the uniform size of sp^2 carbon domains and red-emissive solid-state CNPs was designed in terms of a framework, linker, and luminescent group using L-cysteine, HEDTA, tartaric acid, and CuCl, as shown in Scheme 1. For the framework, a $[Cu(EDTA)]^+$ complex formed a nonrandom replicating stereoscopic sp^2 carbon domain framework of CNPs. For the linker, tartaric acid was employed between the luminescent groups and the framework or between frameworks. It has been reported that the Cu(I)S complex emits red fluorescence based on the interaction between soft-donor-ligand thiol side groups.[34] Therefore, for the luminescent group, it is desirable to achieve the red emission by modifying the surfaces of the CNPs with a Cu(I)-cysteine complex as the red luminescent group. It has also been reported that metal−cysteine hollow spheres with a liposome-like structure could be fabricated through template-free self-assembly at room temperature.[35] Molecular self-assembly is a process in which a disordered system of pre-existing amphiphilic molecules forms an organized structure without external direction.[36] And liposomes, artificially prepared vesicles made of amphiphilic lipid bilayers by self-assembly technology with various surface functionalized groups, have been popularly utilized in science, industry, and medicine now.[37,38] A Cu^+−cysteine liposome-like system was carefully applied to form hollow sphere structures by self-assembly. The hollow spherical structure enables precise control of the morphology of the CNPs and an increase in the number of luminescent groups available owing to the increase of specific surface area. It is noteworthy that the interior surfaces of the CNPs effectively inhibit aggregation owing to a lack of access to other CNPs without any passivator. Thus, carbonizing the Cu^+−cysteine complex liposome can achieve efficient solid-state emitting HTLCu-CNPs.

3.2. Characterization of HTLCu-CNPs. In this work, a one-pot microwave-assisted pyrolysis method was used to prepare the CNPs. This method was reported as being an effective approach for preparing blue- or green-emissive CNPs in our previous work.[39,40] Here, the CNPs were prepared by microwave-assisted pyrolysis of HEDTA, tartaric acid, L-cysteine, and a CuCl solution. Figure 1a shows the TEM images of the HTLCu-CNPs. The images clearly reveal that the HTLCu-CNPs are hollow sphere structures with a relatively narrow size distribution (inset of Figure 1a). The average

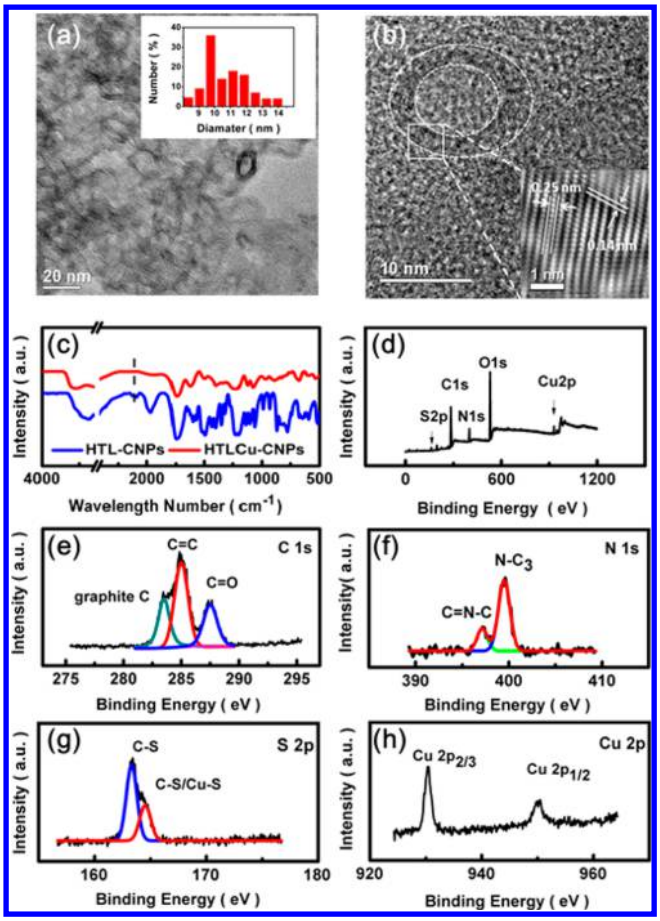

Figure 1. (a) TEM image and size distribution of the HTLCu-CNPs. (b) HRTEM image of the HTLCu-CNPs. A scale bar of 20 nm is shown in the TEM images. A scale bar of 1 nm is shown in the HRTEM image in the inset of panel b. (c) FTIR spectra of the HTL-CNPs (blue line) and HTLCu-CNPs (red line). (d) Overall XPS spectra and detailed XPS spectra of (e) C 1s, (f) N 1s, (g) S 2p, and (h) Cu 2p of HTLCu-CNPs.

particle size was approximately 10 nm. The high-resolution TEM (HRTEM) image (Figure 1b) shows a hollow HTLCu-CNP with resolved, highly ordered crystalline lattice fringes. The thickness of the carbon shell was approximately 2.65 ± 0.45 nm. A representative HRTEM image (inset of Figure 1b) displays clear lattice spacings of 0.14 and 0.25 nm which correspond to the typical carbon−carbon distance of 0.14 nm[41] and the (100) diffraction plane of graphite, respectively.[42] The above results suggest that the HTLCu-CNPs were composed of highly ordered graphite-like carbon atoms.

The surface functional groups on the surfaces of the HTLCu-CNPs were detected by FTIR, and the results are seen in Figure 1c. The broad absorption bands show the presence of ν (O−H) and ν (N−H) at 3300−3650 cm^{-1}, γ (C−H) at 3000 cm^{-1}, ν (S−H) at 2100 cm^{-1}, ν (−C═O) at 1741 cm^{-1}, ν (C−S and C−N) at 1124 and 1500 cm^{-1}, respectively, ν (C═C) at 1616 cm^{-1}, and ν (C−N) at 1580 cm^{-1} (amide II). In addition, the peaks at 1400, 1227, and 1077 cm^{-1} correspond to the asymmetric and symmetric stretching vibrations of C−O−C, respectively. The CNPs prepared without CuCl (HTL-CNPs) were also fabricated and characterized for comparison (blue line). The S−H peak in the HTL-CNPs at 2100 cm^{-1} disappeared in the HTLCu-CNPs (red line), indicating that L-cysteine bound with Cu^+ ions completely.

DOI: 10.1021/acsami.6b10654
ACS Appl. Mater. Interfaces 2016, 8, 31863−31870

To understand the chemical composition of the HTLCu-CNPs, a sequence of XPS spectra is shown in Figure 1d. There are five peaks located at approximately 163, 285, 399, 530, and 930 eV corresponding to S 2p, C 1s, O 1s, N 1s, and Cu 2p, respectively. The C 1s analysis (Figure 1e) reveals three different types of carbon atoms: graphite (C═C/C−C, 283.5 and 284.7 eV), C═O (286.6 eV), and C−O (287.5 eV). Unlike many other reported CNPs,[6,20,43] the sharp peak at 283.5 eV corresponding to graphite-phase carbon originates from the carbonization framework of $[Cu(EDTA)]^+$. This clearly indicates that the conjugated sp^2 carbon domains in the CNPs were achieved, resulting in formation of a periodic graphite structure in the CNPs, as demonstrated by the HRTEM image in Figure 1b. The peak centered at 397.8 eV (Figure 1f) in the N 1s spectrum is attributed to the two chemically nonequivalent N atoms of the molecule, similar to phthalocyine.[44] The two peaks located at 163.4 and 164.6 eV in the S 2p spectrum (Figure 1g) are assigned to the $2p_{3/2}$ and $2p_{1/2}$ positions, respectively, of the C−S covalent bond.[11] Two peaks located at slightly lower binding energies (930.5 and 950.3 eV) in Figure 1h are assigned to the $2p_{3/2}$ and $2p_{1/2}$ positions, respectively, of elemental Cu, which coincides with the Cu^+ oxidation state, as opposed to the peak at 933.8 eV expected for the Cu^{2+} oxidation state.[45] The XPS spectra of the HTL-CNPs are shown in Figure S1. The similar peak at 283.5 eV indicates the existence of graphite-phase carbon.

In Figure S2, the UV−vis absorption spectrum of the HLTCu-CNPs shows an obvious optical absorption edge in the UV region with a tail extending to the visible region. A broad weak absorption peak at approximately 310 nm is attributed to the $\pi \rightarrow \pi^*$ transition of the bending of the graphite-like carbon sheets (sp^2 carbon domains) into the surfaces of the CNPs,[46] in perfect accordance with the HRTEM and XPS results.

3.3. Red and Blue Luminescence of HTLCu-CNPs and HTLM-CNPs. Figure 2 shows the PL spectra of the HTLCu-CNPs, which exhibit an almost excitation wavelength-independent PL peak centered at 620 nm under excitation wavelengths from 340 to 500 nm. This excitation wavelength-independent characteristic is quite different from the excitation wavelength characteristics of most known CNPs. The strongest emission of the HTLCu-CNPs is centered at 620 nm under 380 nm light excitation, and their PL QY is 17%. To further investigate the origin of the CNP fluorescence, the fluorescence lifetime of the HTLCu-CNPs was measured and is compared in Figure S3 and Table S1. The PL decay curve of the red emissions in the HTLCu-CNPs is biexponential with an average PL lifetime of 10.44 μs. The relatively long excited-state lifetime in the microsecond range suggests that the low-energy emission is most likely associated with the spin-forbidden transition of the triplet parentage of copper(I)−thiolate complexes.[34] Without Cu^+ ion in original materials, HTL-CNPs exhibited a blue fluorescence peak, as shown in Figure S4, with an average PL lifetime of 5.45 ns, as shown in Figure S5. Such a short lifetime in HTL-CNPs in the nanosecond range, similar to that of other carbon dots,[12,47,48] was attributed to the radiative recombination nature.[49] As demonstrated in Figure S6, the HTL-CNPs showed an obvious absorption band centered at 352 nm in the UV−vis absorption spectrum.

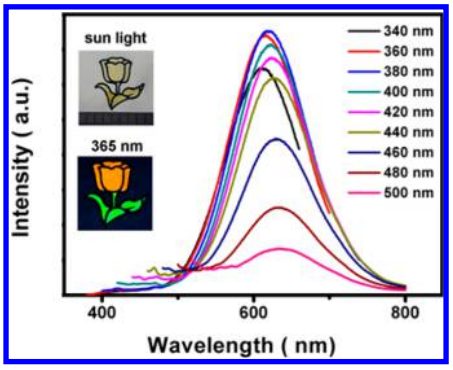

Figure 2. PL emission spectra of the HTLCu-CNPs under different excitation wavelengths. Hand-painted flower photographs painted with HTLCu-CNPs and green-emissive CNPs under visible (top) and 365 nm (bottom) light irradiation are shown in the inset of this figure.

The energy level diagram of Cu(I) d orbital (left), HTL-CNPs ligand (right), and HTLCu-CNPs (middle) is shown in Scheme 2 to explain the mechanism of red-light emission. The Cu(I)-based complex CNP has a full d orbital (d^{10}) in the central copper ion, and its d orbital is easily distorted by ligands. In Figure S2, the strong absorption band peaked at around 310 nm originates from a $d\pi-\pi^*$ transition of the bending of graphite-like carbon sheets, as shown by a blue line in Scheme 2. As a consequence, the HTLCu-CNP exhibits a red emission band of 620 nm from a metal-to-ligand-charge-transfer (MLCT)[50] transition, as shown by a red line, having an excited-state lifetime in the range of microseconds. In contrast, the HTL-CNP ligands just have a blue emission band of 475 nm with a several nanoseconds, as summarized in Table S1.

Scheme 2. Energy Level Diagram of Cu(I) d Orbital (Left), HTL-CNP Ligands (right), and HTLCu-CNPs (Middle)

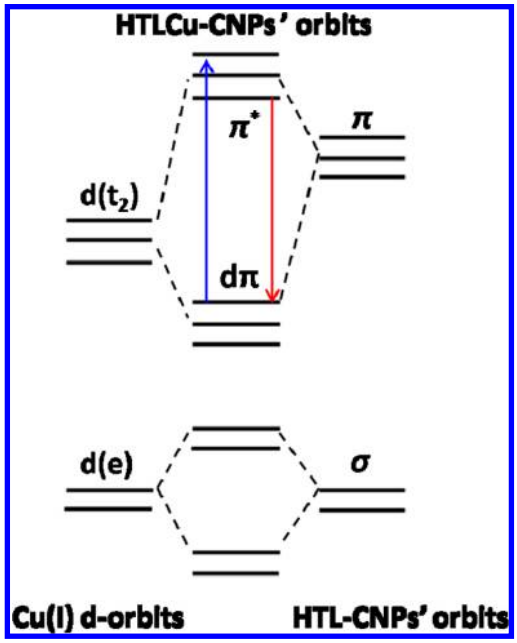

HEDTA is a strong metal ion chelator with a stable stereochemical structural formula.[51] The actual size of sp^2 carbon domains in the CNPs can be considered to be the diameter of the $[Cu(EDTA)]^+$ complex molecule. The homogeneity for the size of true sp^2 carbon domains in HTL-CNPs is very important to determine an excitation wavelength-independent emission in HTLCu-CNPs. This means that the HTLCu-CNPs have the similar energy levels

DOI: 10.1021/acsami.6b10654
ACS Appl. Mater. Interfaces 2016, 8, 31863−31870

of dπ, resulting in an efficient charge transfer process from Cu(I) to HTL-CNPs.

According to previous works, the Cu^{+} ions significantly influence the PL behavior of thiolate-ligated compounds; this is apparently also the case in our experiment. The effects of Cu^{2+}, Fe^{2+}, Fe^{3+}, Ag^{+}, Mn^{2+}, Zn^{2+}, and Cd^{2+} doping into the HLT-CNPs were also investigated, as shown in Figure 3. All the

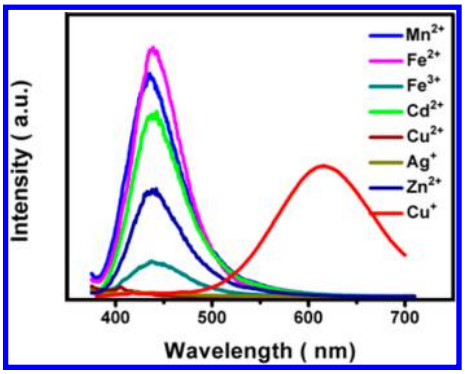

Figure 3. PL emission spectra of the HTLM-CNPs (M = Mn^{2+}, Fe^{2+}, Fe^{3+}, Cd^{2+}, Cu^{2+}, Ag^{+}, and Zn^{2+}) under 380 nm excitation.

metal-doped CNPs exhibited emission peaks at approximately 475 nm under 380 nm light irradiation, except for the Cu^{+}-doped CNPs. The PL of the HTL-CNPs is completely quenched by either Cu^{2+} or Ag^{+} ions. It is known that the above-mentioned metal-complex-CNPs in this work, except for HTLCu-CNPs, exhibited an onset electronic transitions of $\pi-\pi^{*}$ due to their partially filled d orbitals in their metal ions. In this case, their PL is attributed to the emission from HTL-CNPs ligand. On the other hand, this emission may be quenched by the metal d-d transition, more or less. These observations indicate that this approach may be used for PL on/off detection of Cu^{+}/Cu^{2+}.

It was found that the as-prepared HTLCu-CNPs were unstable in a humid environment, which is also the common shortcoming for most CNPs. As we know, organosilane-functionalized CNPs can optimize both the QY and the PL lifetime of the CNPs.[52,53] In this work, to improve the emission efficiency, moisture resistance, and stabilization, SiHTLCu-CNPs were investigated by mixing precursor HTLCu-CNPs with TEOS before microwave heating. After being organo-silanized, the PL spectra of the SiHTLCu-CNPs were measured and are shown in Figure 4a. The SiHTLCu-CNPs exhibit an emission peak at 667 nm under 360 nm excitation. A QY of 47% was achieved because of the inhibition of aggregation-induced fluorescence quenching, which is the highest value recorded for red-emissive solid-state carbon-based nanomaterials. As compared to the HTLCu-CNPs, the PL of the SiHTLCu-CNPs shows a 47 nm red-shift, which may be attributed to the greater number of surface defects[52] on CNPs that originated from the interaction between various reactive intermediates on the surface and the TEOS network-modified CNP surface. Such a change consequently narrowed the energy levels, as demonstrated by the blue-shifted UV−vis absorption spectra (Figure S2), and caused the red-shift of the PL emission of the HTLCu-CNPs.[54] Photographs of SiHTLCu-CNP phosphors under 365 (top) and 460 nm (bottom) light irradiation are shown in the inset of Figure 4a. Figure 4b shows the dependence of the PL intensity and emission wavelength on excitation wavelength. Interestingly, the PL intensity ratio of

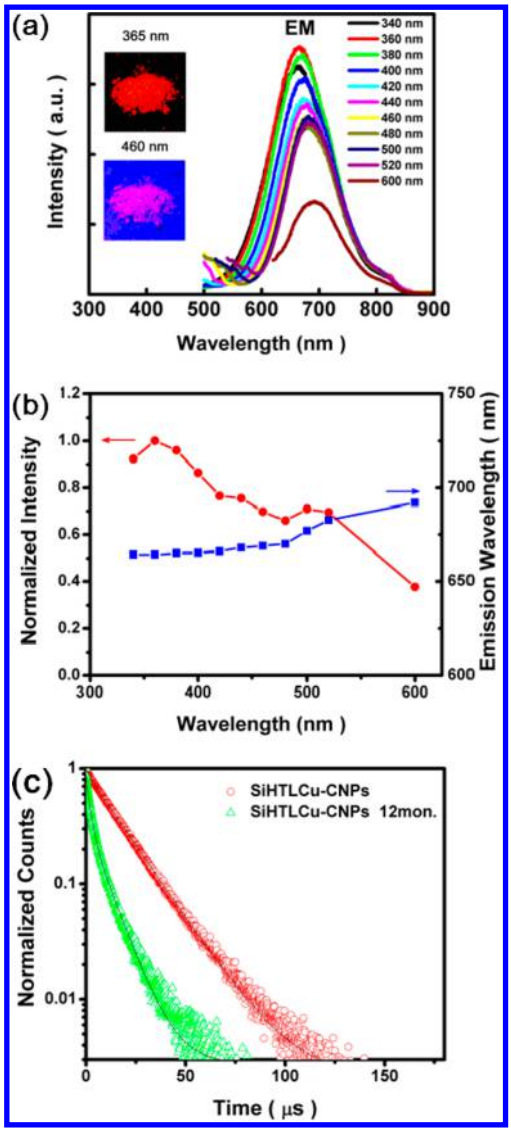

Figure 4. (a) PL spectra of the SiCNPs-CNPs. Insets: Photographs of the SiCNPs-CNP powders under 365 nm UV light (top) and 460 nm LED lamp (bottom). (b) Dependence of normalized PL intensity (red) and emission wavelength (blue) on excitation wavelength. (c) PL decay curves collected at 660 nm for the SiHTLCu-CNPs before and after storage in air for 12 months.

460 to 360 nm in the SiHTLCu-CNPs remained 70%. Thus, luminescent CNPs can be potentially applied to commercial WLEDs based on a 460 nm emissive GaN-based chip. Amazingly, the SiHTLCu-CNPs showed excellent stability, revealing a PL QY of 25% after storage in air for 12 months. As compared to the as-prepared SiHTLCu-CNPs, the emission wavelength after 12 months of storage showed almost no change. It remained the same emission peak centered at 663 nm under 360 nm light excitation (Figure S7). The PL decay curves collected at 663 nm for the SiHTLCu-CNPs before and after storage in air for 12 months are shown in Figure 4c, and the parameters are listed in Table 1. The PL decay curve from the SiHTLCu-CNPs phosphor is biexponential, and the average lifetimes of the SiHTLCu-CNPs before and after storage in air for 12 months are 16.86 and 7.39 μs, respectively, which are of the same order of magnitude as HTLCu-CNPs, indicating that red-emissive SiHTLCu-CNPs are derived from HTLCu-CNPs.

DOI: 10.1021/acsami.6b10654
ACS Appl. Mater. Interfaces 2016, 8, 31863−31870

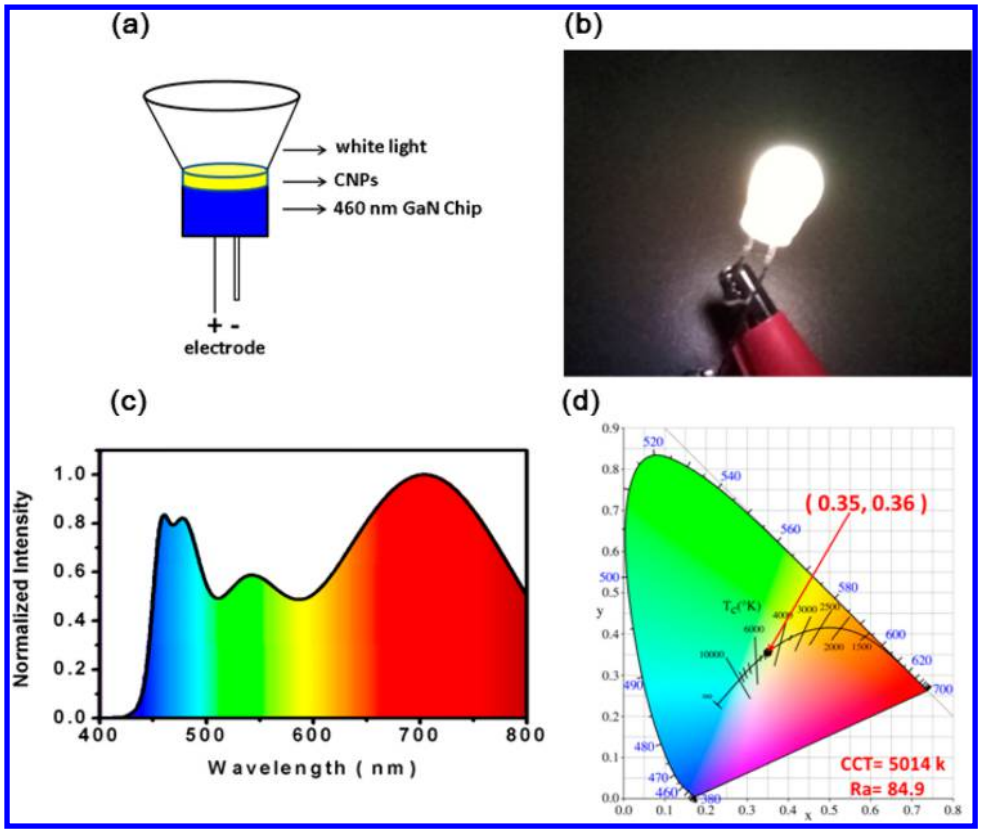

Figure 5. Scheme of WLED fabricated by depositing SiHTLCu-CNPs and green-emissive CNPs phosphors onto a 460 nm blue GaN-based chip. (a) Fabrication strategy of WLEDs based on 460 nm light-emitting diodes. (b) Photograph of the working WLED. (c) Emission spectrum and (d) color coordinates of the WLED.

However, the silanization slowed the CNPs from oxidation and improved the stability of our CNPs.

To fabricate WLEDs, SiHTLCu-CNPs mixed with green-emissive solid-state CNPs (centered at 550 nm under 460 nm excitation, PL QY of 23%, see Figure S8) were employed as phosphors. They were deposited onto a 460 nm GaN LED. The scheme and working photograph of the WLED are shown in Figures 5a and b, respectively. The lighting characteristics of the WLED were measured, and its emission spectrum is shown in Figure 5c. The peak occurring around 480 nm is derived from the shoulder peak of the green-emissive CNPs at 480 nm, as shown in Figure S8. White-light emission was obtained by introducing the red and green CNP phosphors, and the emission spectrum shows a wide range from 460 to 900 nm. The CIE coordinates are shown in Figure 5d. The CIE coordinates of the WLED are (0.35, 0.36), which is close to pure white light (0.33, 0.33), and the correlated color temperature (CCT) is 5014 K, indicating that the red-emissive solid-state CNPs have potential application in white lighting.

4. CONCLUSIONS

In summary, efficient and stable red-emissive solid-state CNPs with highly ordered graphite-like structures for WLEDs were designed and prepared by molecular self-assembly and microwave-assisted pyrolysis. The red emission originated from the red luminescent group of a Cu^{+}−cysteine complex, which was confirmed by PL spectroscopy. Moreover, different metal cations were doped into the blue-emissive HTL-CNPs, while only Cu^{+}-doped CNPs exhibited red emission. The HTLCu-CNPs showed a red emissive peak at 620 nm with excitation wavelength independence under excitation of 380 nm UV light. After organosilane functionalization, the PL QY of the SiHTLCu-CNPs was as high as 47%, which is the highest value recorded for red-emissive solid-state CNPs under UV light excitation. Importantly, the SiHTLCu-CNPs showed excellent stability, revealing a PL QY of 25% after storage in air for one year. The efficient red-emissive solid-state CNPs were used to prepare a WLED which exhibited a CIE of (0.35, 0.36) and a CCT of 5014 K. In a word, the development of an effective strategy to produce high-QY red-emissive solid-state CNPs for low-cost colorful illumination under a single light source opens a new path for the commercial application of CNPs.

■ ASSOCIATED CONTENT

Supporting Information

This material is available free of charge via the Internet The Supporting Information is available free of charge on the ACS Publications website at DOI: 10.1021/acsami.6b10654.

XPS spectra of the HTL-CNPs, UV−vis absorption spectrum of the HTLCu-CNPs and SiHTLCu-CNPs, PL decay curves of the HTLCu-CNPs, PL excitation and emission spectra, PL decay curves and UV−vis absorption spectra of HTL-CNPs, fluorescence lifetimes of HTL-CNPs and HTLCu-CNPs, PL emission spectra of SiHTLCu-CNPs under different excitation wavelengths after storage in air for 12 months, and PL excitation and emission spectra of green-emissive CNPs (PDF)

DOI: 10.1021/acsami.6b10654
ACS Appl. Mater. Interfaces 2016, 8, 31863−31870

AUTHOR INFORMATION

Corresponding Authors

*E-mail: guoxy@ciomp.ac.cn.
*E-mail: liuxy@ciomp.ac.cn.

ORCID

Ying Lv: 0000-0003-1649-5258
Xingyuan Liu: 0000-0002-9681-1646

Notes

The authors declare no competing financial interest.

ACKNOWLEDGMENTS

This work was supported by the CAS Innovation Program, the National Natural Science Foundation of China (Grants 61106057, 6140031454, 11504367, and 51503196), the Jilin Province Science and Technology Research Project (Grants 20140520119JH, 20150101039JC, 20160520176JH, and 20160520092JH), and the project of State Key Laboratory of Luminescence and Applications

REFERENCES

(1) Sun, Y. P.; Zhou, B.; Lin, Y.; Wang, W.; Fernando, K. A.; Pathak, P.; Meziani, M. J.; Harruff, B. A.; Wang, X.; Wang, H.; Luo, P. G.; Yang, H.; Kose, M. E.; Chen, B.; Veca, L. M.; Xie, S. Y. Quantum-Sized Carbon Dots for Bright and Colorful Photoluminescence. *J. Am. Chem. Soc.* **2006**, *128*, 7756−7757.

(2) Li, X.; Liu, Y.; Song, X.; Wang, H.; Gu, H.; Zeng, H. Intercrossed Carbon Nanorings with Pure Surface States as Low-Cost and Environment-Friendly Phosphors for White-Light-Emitting Diodes. *Angew. Chem., Int. Ed.* **2015**, *54*, 1759−1764.

(3) Zhang, X. Y.; Zhang, Y.; Wang, Y.; Kalytchuk, X.; Kershaw, S. V.; Wang, Y. H.; Wang, P.; Zhang, T. Q.; Zhao, Y.; Zhang, H. Z.; Cui, T.; Wang, Y. D.; Zhao, J.; Yu, W. W.; Rogach, A. L. Color-Switchable Electroluminescence of Carbon Dot Light-Emitting Diodes. *ACS Nano* **2013**, *7*, 11234−11241.

(4) Mehta, V. N.; Jha, S.; Kailasa, S. K. One-Pot Green Synthesis of Carbon Dots by Using Saccharum Officinarum Juice for Fluorescent Imaging of Bacteria (Escherichia Coli) and Yeast (Saccharomyces Cerevisiae) Cells. *Mater. Sci. Eng., C* **2014**, *38*, 20−27.

(5) Lou, Q.; Qu, S. N.; Jing, P. T.; Ji, W. Y.; Li, D.; Cao, J. S.; Zhang, H.; Liu, L.; Zhao, J. L.; Shen, D. Z. Water-Triggered Luminescent "Nano-Bombs" Based on Supra-(Carbon Nanodots). *Adv. Mater.* **2015**, *27*, 1389−1394.

(6) Zhu, S.; Meng, Q.; Wang, L.; Zhang, J.; Song, Y.; Jin, H.; Zhang, K.; Sun, H.; Wang, H.; Yang, B. Highly Photoluminescent Carbon Dots for Multicolor Patterning, Sensors, and Bioimaging. *Angew. Chem., Int. Ed.* **2013**, *52*, 3953−3957.

(7) Tian, J.; Leng, Y. H.; Zhao, Z. H.; Xia, Y.; Sang, Y. H.; Hao, P.; Zhan, J.; Li, M. C.; Liu, H. Carbon Quantum Dots/Hydrogenated TiO_2 Nanobelt Heterostructures and Their Broad Spectrum Photocatalytic Properties under Uv, Visible, and near-Infrared Irradiation. *Nano Energy* **2015**, *11*, 419−427.

(8) Briscoe, J.; Marinovic, A.; Sevilla, M.; Dunn, S.; Titirici, M. Biomass-Derived Carbon Quantum Dot Sensitizers for Solid-State Nanostructured Solar Cells. *Angew. Chem., Int. Ed.* **2015**, *54*, 4463−4468.

(9) Zhang, H. M.; Wang, Y.; Liu, P. R.; Li, Y. B.; Yang, H. G.; An, T. C.; Wong, P. K.; Wang, D.; Tang, Z. Y.; Zhao, H. J. A Fluorescent Quenching Performance Enhancing Principle for Carbon Nanodot-Sensitized Aqueous Solar Cells. *Nano Energy* **2015**, *13*, 124−130.

(10) Nie, H.; Li, M. J.; Li, Q. S.; Liang, S. J.; Tan, Y. Y.; Sheng, L.; Shi, W.; Zhang, S. X. A. Carbon Dots with Continuously Tunable Full-Color Emission and Their Application in Ratiometric Ph Sensing. *Chem. Mater.* **2014**, *26*, 3104−3112.

(11) Ding, H.; Wei, J.-S.; Xiong, H.-M. Nitrogen and Sulfur Co-Doped Carbon Dots with Strong Blue Luminescence. *Nanoscale* **2014**, *6*, 13817−13823.

(12) Wu, M. B.; Wang, Y.; Wu, W. T.; Hu, C.; Wang, X. N.; Zheng, J. T.; Li, Z. T.; Jiang, B.; Qiu, J. S. Preparation of Functionalized Water-Soluble Photoluminescent Carbon Quantum Dots from Petroleum Coke. *Carbon* **2014**, *78*, 480−489.

(13) Wang, L.; Zhu, S. J.; Wang, H. Y.; Qu, S. N.; Zhang, Y. L.; Zhang, J. H.; Chen, Q. D.; Xu, H. L.; Han, W.; Yang, B.; Sun, H. B. Common Origin of Green Luminescence in Carbon Nanodots and Graphene Quantum Dots. *ACS Nano* **2014**, *8*, 2541−2547.

(14) Huang, J. J.; Zhong, Z. F.; Rong, M. Z.; Zhou, X.; Chen, X. D.; Zhang, M. Q. An Easy Approach of Preparing Strongly Luminescent Carbon Dots and Their Polymer Based Composites for Enhancing Solar Cell Efficiency. *Carbon* **2014**, *70*, 190−198.

(15) Lou, Q.; Qu, S.; Jing, P.; Ji, W.; Li, D.; Cao, J.; Zhang, H.; Liu, L.; Zhao, J.; Shen, D. Water-Triggered Luminescent "Nano-Bombs" Based on Supra-(Carbon Nanodots). *Adv. Mater.* **2015**, *27*, 1389−94.

(16) Zhang, W.; Dai, D.; Chen, X.; Guo, X.; Fan, J. Red Shift in the Photoluminescence of Colloidal Carbon Quantum Dots Induced by Photon Reabsorption. *Appl. Phys. Lett.* **2014**, *104*, 091902.

(17) Han, B.; Wang, W.; Wu, H.; Fang, F.; Wang, N.; Zhang, X.; Xu, S. Polyethyleneimine Modified Fluorescent Carbon Dots and Their Application in Cell Labeling. *Colloids Surf., B* **2012**, *100*, 209−214.

(18) Qu, D.; Zheng, M.; Li, J.; Xie, Z.; Sun, Z. Tailoring Color Emissions from N-Doped Graphene Quantum Dots for Bioimaging Applications. *Light: Sci. Appl.* **2015**, *4*, e364.

(19) Jiang, K.; Sun, S.; Zhang, L.; Lu, Y.; Wu, A.; Cai, C.; Lin, H. Red, Green, and Blue Luminescence by Carbon Dots: Full-Color Emission Tuning and Multicolor Cellular Imaging. *Angew. Chem., Int. Ed.* **2015**, *54*, 5360−5363.

(20) Qu, S.; Zhou, D.; Li, D.; Ji, W.; Jing, P.; Han, D.; Liu, L.; Zeng, H.; Shen, D. Toward Efficient Orange Emissive Carbon Nanodots through Conjugated Sp(2) -Domain Controlling and Surface Charges Engineering. *Adv. Mater.* **2016**, *28*, 3516−3521.

(21) Li, Q.; Ohulchanskyy, T. Y.; Liu, R. L.; Koynov, K.; Wu, D. Q.; Best, A.; Kumar, R.; Bonoiu, A.; Prasad, P. N. Photoluminescent Carbon Dots as Biocompatible Nanoprobes for Targeting Cancer Cells in Vitro. *J. Phys. Chem. C* **2010**, *114*, 12062−12068.

(22) Li, H.; He, X.; Kang, Z.; Huang, H.; Liu, Y.; Liu, J.; Lian, S.; Tsang, C. H.; Yang, X.; Lee, S. T. Water-Soluble Fluorescent Carbon Quantum Dots and Photocatalyst Design. *Angew. Chem., Int. Ed.* **2010**, *49*, 4430−4434.

(23) Jiang, K.; Sun, S.; Zhang, L.; Lu, Y.; Wu, A.; Cai, C.; Lin, H. Red, Green, and Blue Luminescence by Carbon Dots: Full-Color Emission Tuning and Multicolor Cellular Imaging. *Angew. Chem., Int. Ed.* **2015**, *54*, 5360−5363.

(24) Hu, S.; Trinchi, A.; Atkin, P.; Cole, I. Tunable Photoluminescence across the Entire Visible Spectrum from Carbon Dots Excited by White Light. *Angew. Chem., Int. Ed.* **2015**, *54*, 2970−2974.

(25) Pan, D.; Zhang, J.; Li, Z.; Zhang, Z.; Guo, L.; Wu, M. Blue Fluorescent Carbon Thin Films Fabricated from Dodecylamine-Capped Carbon Nanoparticles. *J. Mater. Chem.* **2011**, *21*, 3565−3567.

(26) Qu, S. N.; Wang, X. Y.; Lu, Q. P.; Liu, X. Y.; Wang, L. J. A Biocompatible Fluorescent Ink Based on Water-Soluble Luminescent Carbon Nanodots. *Angew. Chem., Int. Ed.* **2012**, *51*, 12215−12218.

(27) Chen, P. C.; Chen, Y. N.; Hsu, P. C.; Shih, C. C.; Chang, H. T. Photoluminescent Organosilane-Functionalized Carbon Dots as Temperature Probes. *Chem. Commun.* **2013**, *49*, 1639−1641.

(28) Deng, Y.; Zhao, D.; Chen, X.; Wang, F.; Song, H.; Shen, D. Long Lifetime Pure Organic Phosphorescence Based on Water Soluble Carbon Dots. *Chem. Commun.* **2013**, *49*, 5751−5753.

(29) Chen, B.; Feng, J. C. White-Light-Emitting Polymer Composite Film Based on Carbon Dots and Lanthanide Complexes. *J. Phys. Chem. C* **2015**, *119*, 7865−7872.

(30) Li, H.; Kang, Z.; Liu, Y.; Lee, S.-T. Carbon Nanodots: Synthesis, Properties and Applications. *J. Mater. Chem.* **2012**, *22*, 24230.

(31) Zhou, Y.; Xing, G.; Chen, H.; Ogawa, N.; Lin, J. M. Carbon Nanodots Sensitized Chemiluminescence on Peroxomonosulfate-Sulfite-Hydrochloric Acid System and Its Analytical Applications. *Talanta* **2012**, *99*, 471−477.

DOI: 10.1021/acsami.6b10654
ACS Appl. Mater. Interfaces 2016, 8, 31863−31870

(32) Bhunia, S. K.; Saha, A.; Maity, A. R.; Ray, S. C.; Jana, N. R. Carbon Nanoparticle-Based Fluorescent Bioimaging Probes. *Sci. Rep.* **2013**, *3*, 1473.
(33) Dong, X.; Wei, L.; Su, Y.; Li, Z.; Geng, H.; Yang, C.; Zhang, Y. Efficient Long Lifetime Room Temperature Phosphorescence of Carbon Dots in a Potash Alum Matrix. *J. Mater. Chem. C* **2015**, *3*, 2798−2801.
(34) Yam, V. W.-W.; Lam, C.-H.; Fung, W. K.-M.; Cheung, K.-K. Syntheses, Photophysics, and Photochemistry of Trinuclear Copper(I) Thiolate and Hexanuclear Copper(I) Selenolate Complexes: X-Ray Crystal Structures of [Cu6(M-Dppm)4(M3-Seph)4](Bf4)2 and [Cu6{M-(Ph2p)2nh}4(M3-Seph)4](Bf4)2. *Inorg. Chem.* **2001**, *40*, 3435−3442.
(35) Caoa, C. B.; An, X. Q.; Yu, X. L.; Ma, X. L. Preparation of Ni-Cysteine Hollow Spheres with Ferromagnetic Property and Good Biocompatibility. *Curr. Nanosci.* **2010**, *6*, 592−597.
(36) Ariga, K.; Yamauchi, Y.; Rydzek, G.; Ji, Q.; Yonamine, Y.; Wu, K. C. W.; Hill, J. P. Layer-by-Layer Nanoarchitectonics: Invention, Innovation, and Evolution. *Chem. Lett.* **2014**, *43*, 36−68.
(37) Al-Jamal, W. T.; Kostarelos, K. Liposomes: From a Clinically Established Drug Delivery System to a Nanoparticle Platform for Theranostic Nanomedicine. *Acc. Chem. Res.* **2011**, *44*, 1094−1104.
(38) Ling, H.; Fabbri, M.; Calin, G. A. Micrornas and Other Non-Coding Rnas as Targets for Anticancer Drug Development. *Nat. Rev. Drug Discovery* **2013**, *12*, 847−865.
(39) Zhang, Y.; Hu, Y.; Lin, J.; Fan, Y.; Li, Y.; Lv, Y.; Liu, X. Excitation Wavelength Independence: Toward Low-Threshold Amplified Spontaneous Emission from Carbon Nanodots. *ACS Appl. Mater. Interfaces* **2016**, *8*, 25454−25460.
(40) Qu, S. N.; Liu, X. Y.; Guo, X. Y.; Chu, M. H.; Zhang, L. G.; Shen, D. Z. Amplified Spontaneous Green Emission and Lasing Emission from Carbon Nanoparticles. *Adv. Funct. Mater.* **2014**, *24*, 2689−2695.
(41) Suenaga, K.; Wakabayashi, H.; Koshino, M.; Sato, Y.; Urita, K.; Iijima, S. Imaging Active Topological Defects in Carbon Nanotubes. *Nat. Nanotechnol.* **2007**, *2*, 358−360.
(42) Baker, S. N.; Baker, G. A. Luminescent Carbon Nanodots: Emergent Nanolights. *Angew. Chem., Int. Ed.* **2010**, *49*, 6726−6744.
(43) Bao, L.; Zhang, Z. L.; Tian, Z. Q.; Zhang, L.; Liu, C.; Lin, Y.; Qi, B.; Pang, D. W. Electrochemical Tuning of Luminescent Carbon Nanodots: From Preparation to Luminescence Mechanism. *Adv. Mater.* **2011**, *23*, 5801−5806.
(44) Ahlund, J.; Nilson, K.; Schiessling, J.; Kjeldgaard, L.; Berner, S.; Martensson, N.; Puglia, C.; Brena, B.; Nyberg, M.; Luo, Y. The Electronic Structure of Iron Phthalocyanine Probed by Photoelectron and X-Ray Absorption Spectroscopies and Density Functional Theory Calculations. *J. Chem. Phys.* **2006**, *125*, 34709.
(45) El-Deab, M. S. Interaction of Cysteine and Copper Ions on the Surface of Iron: Eis, Polarization and Xps Study. *Mater. Chem. Phys.* **2011**, *129*, 223−227.
(46) Das, B.; Dadhich, P.; Pal, P.; Srivas, P. K.; Bankoti, K.; Dhara, S. Carbon Nanodots from Date Molasses: New Nanolights for the in Vitro Scavenging of Reactive Oxygen Species. *J. Mater. Chem. B* **2014**, *2*, 6839−6847.
(47) Ghosh, S.; Chizhik, A. M.; Karedla, N.; Dekaliuk, M. O.; Gregor, I.; Schuhmann, H.; Seibt, M.; Bodensiek, K.; Schaap, I. A. T.; Schulz, O.; Demchenko, A. P.; Enderlein, J.; Chizhik, A. I. Photoluminescence of Carbon Nanodots: Dipole Emission Centers and Electron-Phonon Coupling. *Nano Lett.* **2014**, *14*, 5656−5661.
(48) Qian, Z. S.; Shan, X. Y.; Chai, L. J.; Ma, J. J.; Chen, J. R.; Feng, H. Si-Doped Carbon Quantum Dots: A Facile and General Preparation Strategy, Bioimaging Application, and Multifunctional Sensor. *ACS Appl. Mater. Interfaces* **2014**, *6*, 6797−6805.
(49) Zhu, H.; Wang, X. L.; Li, Y. L.; Wang, Z. J.; Yang, F.; Yang, X. R. Microwave Synthesis of Fluorescent Carbon Nanoparticles with Electrochemiluminescence Properties. *Chem. Commun.* **2009**, 5118−5120.
(50) Garakyaraghi, S.; Danilov, E. O.; McCusker, C. E.; Castellano, F. N. Transient Absorption Dynamics of Sterically Congested Cu(I) Mlct Excited States. *J. Phys. Chem. A* **2015**, *119*, 3181−3193.
(51) Nette, D.; Seubert, A. Determination of Aminopolycarboxylic Acids at Ultra-Trace Levels by Means of Online Coupling Ion Exchange Chromatography and Inductively Coupled Plasma-Mass Spectrometry with Indirect Detection Via Their Pd^{2+}-Complexes. *Anal. Chim. Acta* **2015**, *884*, 124−132.
(52) Xie, Z.; Wang, F.; Liu, C. Y. Organic-Inorganic Hybrid Functional Carbon Dot Gel Glasses. *Adv. Mater.* **2012**, *24*, 1716−1721.
(53) Ma, L.; Xiang, W.; Gao, H.; Pei, L.; Ma, X.; Huang, Y.; Liang, X. Carbon Dot-Doped Sodium Borosilicate Gel Glasses with Emission Tunability and Their Application in White Light Emitting Diodes. *J. Mater. Chem. C* **2015**, *3*, 6764−6770.
(54) Hou, S.; Kasner, M. L.; Su, S.; Patel, K.; Cuellari, R. Highly Sensitive and Selective Dopamine Biosensor Fabricated with Silanized Graphene. *J. Phys. Chem. C* **2010**, *114*, 14915−14921.

DOI: 10.1021/acsami.6b10654
ACS Appl. Mater. Interfaces 2016, 8, 31863−31870